Title
A stress analysis method for molecular dynamics systems

Authors
Yang, J
Komvopoulos, K

Publication Date
2020-06-01

DOI
10.1016/j.ijsolstr.2020.02.003

Peer reviewed

International Journal of Solids and Structures 193–194 (2020) 98–105

Contents lists available at ScienceDirect

International Journal of Solids and Structures

journal homepage: www.elsevier.com/locate/ijsolstr

A stress analysis method for molecular dynamics systems

J. Yang, K. Komvopoulos*

Department of Mechanical Engineering, University of California, Berkeley, CA 94720, USA

ARTICLE INFO

Article history:
Received 14 October 2019
Revised 27 January 2020
Accepted 1 February 2020
Available online 2 February 2020

Keywords:
Atomic stress
Crystal solids
Deformation
Interatomic potential
Molecular dynamics
Stress analysis

ABSTRACT

As the development of micro/nanoelectromechanical devices continues at a fast pace, there is a growing need to bridge the gap between material behavior at the atomic and molecular levels and material behavior at length scales relevant to most engineering and industrial applications. Since stress is one of the most fundamental quantities in continuum mechanics (CM), it is desirable to introduce stress methods that are applicable to both continuum and discrete systems, such as those modeled by molecular dynamics (MD). Thus, the objective of this study was to demonstrate how a traction vector-based stress method that is compatible with CM can be used to examine MD systems of crystalline solids undergoing small lattice distortion. In the bulk of face-centered-cubic (FCC) and body-centered-cubic solids, the traction vector-based atomic stress definition used in this study is shown to be equivalent to the classical energy-based virial stress that is commonly used for small deformations and low temperatures, i.e., negligible thermal vibration. However, contrary to the virial stress, the components of the present atomic stress diminish in the region close to a free surface, consistent with the traction-free boundary condition. The validity of the stress method developed herein is demonstrated by MD results of the bulk modulus of FCC copper, the surface tension of an FCC solid, and the subsurface stress field of an FCC half-space indented by a rigid flat punch.

1. Introduction

The rapid growth of various nanotechnology and nanoscience sectors has generated high interest in the development of mechanics approaches applicable to the atomic scale, where continuum mechanics (CM) does not hold. For example, fracture mechanics within the framework of continuum theory has been reported to break down at the nanoscale (Shimada et al., 2015), atomic-scale surface roughness has been shown to greatly affect the contact area, stresses, friction force, and lateral contact stiffness predicted by CM theory (Luan and Robbins, 2005), and contact deformation predicted by CM differs significantly from that obtained with atomistic models in the presence of surface adhesion (Solhjoo and Vakis, 2015). Nevertheless, developments in advanced microanalysis techniques and effective computational methods have enabled material characterization and modeling of physical phenomena at the atomic scale. Particularly, molecular dynamics (MD) has been proven an efficient computational method for analyzing atomic-scale deformation, fracture, and phase changes in solids. For instance, atomistic dynamic simulations of single-crystal plasticity have provided insight into the limits of dislocation-mediated plasticity in body-centered-cubic (BCC) tantalum (Zepeda-Ruiz et al., 2017) and large-scale MD simulations have been performed to elucidate temperature- and stress-induced martensite-austenite transformation in equiatomic titanium-nickel shape-memory alloy (Chen et al., 2018). Various computational methods for interfacing large-scale MD simulations with CM models have been used to obtain continuum parameters, e.g., deformation gradient and Cauchy stress, from MD systems by minimizing the difference between identical quantities at the scales of MD and CM models (Zhang et al., 2015), or to recover crystal defects, i.e., dislocations, twin boundaries, and stacking faults (Sansoz, 2011; Stukowski et al., 2010), from the particle-position trajectories in MD models (Stukowski, 2012). New computational techniques have been developed for large-scale atomistic simulations of crystalline solids, including multiscale modeling of structurally-graded materials wherein constitutive material parameters extracted from MD simulations are used to calibrate material processes at the mesoscale by applying discrete dislocation dynamics and then introduce the predicted grain size-dependent stress-strain relations into the crystal plasticity parameters of finite element-based CM models (Saether et al., 2014).

Atomistic simulations of a rigid tip indenting a copper substrate have shown that the resulting elastic stress field bears some similarity to that predicted by classical Hertz theory (Leng et al., 2000). MD simulations have been used to investigate the indentation and scratching behavior of crystalline aluminum

* Corresponding author.
E-mail address: kyriakos@me.berkeley.edu (K. Komvopoulos).

https://doi.org/10.1016/j.ijsolstr.2020.02.003
0020-7683/

(Komanduri et al., 2000) and single-crystal copper (Belak and Stowers, 1992), as well as single and cyclic indentation of metal-like substrates by a diamond-like tip (Komvopoulos and Yan, 1997). In addition, several MD studies have provided insight into various phase change and deformation phenomena, such as the diamond-to-amorphous phase transformation occurring in the near-surface region of indented crystalline silicon (Kallman et al., 1993), the indentation and cutting of Lennard–Jones (LJ) crystalline solids (Hoover et al., 1989), the stress field in a metallic substrate indented by a hard ball or diamond tool (Belak and Stowers, 1990, 1992), the formation of a dislocation in an LJ solid due to a penetrating atom with the dislocation movement coinciding with that predicted by plastic indentation analysis (Yan and Komvopoulos, 1998), the dependence of the friction coefficient on the size, shape, and orientation of a sliding diamond tip (Yang and Komvopoulos, 2005), and the pseudoelastic behavior of nickel-titanium alloy under various monotonic and cyclic loading conditions (Srinivasan et al., 2018; Wang et al., 2017).

Despite of the important insight into atomic-scale deformation and phase change phenomena provided by the foregoing studies and others dealing with deformation processes at the atomic level, scale bridging between MD and CM analyses remains challenging, hindering the simultaneous study of physical processes at the atomic and continuum levels. Specifically, because stress is one of the most fundamental quantities in CM, it is essential to introduce a stress definition applicable to both continuum and discrete systems. The most common stress definition in discrete-particle systems is the virial stress, which is derived from the generalization of the virial theorem (Clausius, 1870) for gas pressure and the solution of the spatial equation of balance of momentum. The virial stress consists of two components: a kinetic component depending on the atomic particle mass and velocity and a potential component depending on the interatomic forces and atom positions (Tsai, 1979). Based on a general stress theorem for quantum mechanical systems (Nielsen and Martin, 1985), an equivalent stress formula was derived for systems in which the total potential energy is only a function of interatomic distance (Vitek and Egami, 1987). A stress definition slightly different from the virial stress has also been used to compute stress components at different surfaces (Cheung and Yip, 1991); however, it was argued that the stress field of a dynamically deforming atomistic particle system that is equivalent to a continuum system depends only on the interatomic forces and that the kinetic component of the virial stress generally results in erroneous stress interpretation (Zhou, 2003). Moreover, it has been reasoned that the virial stress represents an atomistic definition of stress that is equivalent to the continuum Cauchy stress, provided spatial and temporal averages are computed in an Eulerian reference frame (Subramaniyan and Sun, 2008). In the absence of the kinetic component, the virial stress is equivalent to the atomic stress in solids subjected to homogeneous deformation (Born and Huang, 1954) under the assumption that the strain energy is equal to the change in total interatomic potential energy of the system, i.e., the summation of the two-body interatomic potentials of all atom pairs. This stress definition is equivalent to the virial stress at a temperature of 0 K.

Stress definitions equivalent to that of the classical virial stress (Born and Huang, 1954) have been adopted in several atomistic studies. For example, MD simulations were performed to examine the atomic stress field in a gold substrate due to the adhesion, nanoindentation, and detachment of a nickel tip (Landman et al., 1990). Leng et al. (2000) used MD simulations to determine the stress distribution in a face-centered-cubic (FCC) copper substrate due to contact with a rigid copper-like tip and obtained results similar to those derived from classical Hertz theory for purely elastic deformation. However, the nonzero normal and shear stresses at the free surface predicted in the foregoing study are inconsistent with the traction-free boundary condition, suggesting that this atomic stress definition is incompatible with the Cauchy stress definition in the neighborhood of a free surface.

In CM analyses, the stress is defined by traction vectors, i.e., forces acting on unit areas (Love, 1944). This approach may be extended to MD analyses by defining the atomic stress in terms of the forces acting on a unit area. It has been proposed (Scagnetti et al., 1996) that the traction vector acting on an atom can be represented by the resultant vector of all interatomic forces whose trajectories pass through a finite segment of a plane (on which the given atom is centered) divided by the segment area. Stress distributions that are both locally descriptive and relatively smooth can be obtained with a plane size equal to five times the interatomic spacing. However, defining a material plane that contains a few atoms is hindered by numerical complexity introduced by atomic thermal vibration. In addition, accounting for all of the interatomic forces associated with the atoms lying on the particular material surface is cumbersome.

The objective of this study was to introduce a traction vector-based stress method that uses a geometrical plane rather than a material plane to define the atomic stress and examine its equivalence with energy-based atomic stress methods. It is shown that the present stress definition is equivalent to that of the classical virial stress in the bulk of FCC and BCC solids provided the interatomic forces can be characterized by pair potentials and the crystal structure is not grossly distorted. The validity of the stress method introduced in this study is demonstrated by MD simulation results of the bulk modulus of FCC copper, the surface tension of an FCC solid, and the stress field of an FCC substrate indented by a flat diamond tip.

2. Interatomic potential functions

MD is an effective method for calculating instantaneous material properties and analyzing atomic-scale deformation. In MD analyses, the atomic motion is described by Newton's second law and the interatomic forces are determined from a two-body or many-body potential function. The parameters of the interatomic potentials are usually extracted by fitting the material parameters, such as elastic constants, phonon frequencies, and energy of vacancy formation (Foiles et al., 1986; Eggen et al., 1992). A typical two-body potential describes the force acting between two atoms i and j of the system as a function of their interatomic distance r_{ij}, that is, the force is independent of the position of other atoms. Thus, a two-body potential function φ can be mathematically expressed as

$$\varphi_{ij} = \varphi(r_{ij}). \tag{1}$$

If the force acting between atoms i and j is also affected by the neighboring atoms, then it is described by a many-body potential defined as

$$\varphi_{ij\ldots kl} = \varphi(r_{ij}, \ldots, r_{kl}). \tag{2}$$

In the present analysis, a previously developed three-dimensional MD code of atomistic systems characterized by two-body potentials (Komvopoulos and Yan, 1997) was modified according to the objectives of this study. Although the stress definition used in the present analysis is for systems characterized by two-body potential functions, it can also be applied to systems characterized by many-body potential functions with minor modification. In the MD simulations, atomic interaction in an FCC copper-like material is described by the Morse potential given by

$$\varphi(r_{ij}) = De^{-2\alpha(r_{ij}-r_0)} - 2De^{-\alpha(r_{ij}-r_0)}, \tag{3}$$

where $-D$ is the minimum value of the potential (well depth), r_0 is the equilibrium bond distance corresponding to the well depth,

and α is a parameter that controls the potential width (a smaller α implies a deeper well).

For the countersurface, which is modelled as a rigid diamond-like tip, the interfacial potential that describes tip-substrate atomic interaction is represented by an LJ potential given by

$$\varphi(r_{ij}) = 4\varepsilon\left[\left(\frac{\sigma}{r_{ij}}\right)^{12} - \left(\frac{\sigma}{r_{ij}}\right)^{6}\right], \tag{4}$$

where ε is the well depth (a measure of how strong is the attraction between atoms i and j) and σ is the finite distance at which the potential is zero.

3. Atomic stress analysis

As mentioned earlier, the virial stress is defined for a volume v_i that surrounds atom i and is given by (Zhou, 2003)

$$\sigma_i^{ab} = -\frac{1}{v_i}\sum_{j\neq i}\left(M_i V_i^a V_i^b + F_{ij}^a r_{ij}^b\right), \tag{5}$$

where a and b represent the axes of the coordinate system and take values 1, 2, and 3, M_i and V_i are the atomic mass and velocity, respectively, F_{ij} is the interatomic force, and r_{ij}^b represents the scalar components of the distance vector $\boldsymbol{r}_{ij}$. The convention is that a negative stress denotes attraction, whereas a positive stress denotes repulsion. Eq. (5) was also derived in an earlier study (Vitek and Egami, 1987) by using the general stress theorem for quantum mechanical systems (Nielsen and Martin, 1985).

Another commonly used atomic stress definition (Born and Huang, 1954) was obtained by relating the elastic stress to the interatomic potential function of a medium undergoing homogeneous deformation (Egami and Srolovitz, 1982) under the assumption the strain energy equals the change in total interatomic potential energy of the system, i.e., the summation of the two-body interatomic potentials of all atom pairs. Since the interatomic force is defined as

$$F_{ij}^a = -\frac{1}{r_{ij}}\frac{d\varphi}{dr_{ij}}r_{ij}^a, \tag{6}$$

the stress acting on atom i can be written as

$$\sigma_i^{ab} = \frac{1}{v_i}\sum_{j\neq i}\left(\frac{1}{r_{ij}}\frac{d\varphi}{dr_{ij}}r_{ij}^a r_{ij}^b\right), \tag{7}$$

where r_{ij} is the magnitude of the distance vector $\boldsymbol{r}_{ij}$ and ${r_{ij}}^a$ and ${r_{ij}}^b$ are its scalar components in the directions a and b, respectively. Since Eq. (7) is the same as the second term (potential component) of the virial stress (Eq. (5)), the stress definitions given by Eqs. (5) and (7) are equivalent when the temperature is equal to 0 K.

In CM treatments, stress is defined by traction vectors, i.e., the stress components are considered as forces acting on unit surface areas. This concept was extended to the stress analysis of MD systems by introducing an approach that defines stress in terms of the interatomic forces (Scagnetti et al., 1996). The traction vector acting on an atom was obtained as the sum of all interatomic forces whose trajectories cross a finite plane of size equal to about five times the interatomic spacing (on which the reference atom was centered) divided by the plane surface area. However, defining a material surface passing through a few atoms is numerically complex because the surface does not remain planar due to thermal vibration of the atoms. Hence, determining the interatomic forces acting on the atoms of a material surface is nontrivial, especially for edge and corner surface atoms. Therefore, a geometric plane instead of a material surface was used in this study to determine the traction vector acting on each atom of the system.

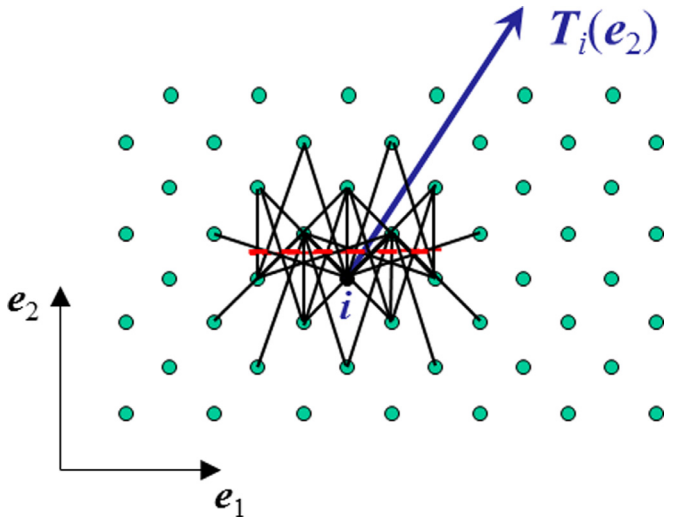

Fig. 1. A 2D schematic illustration of the traction vector calculation at each atom of the system. The red dashed line represents the geometrical plane used to define the atomic stress.

Fig. 1 provides a two-dimensional (2D) schematic description of the calculation of the traction vector $\boldsymbol{T}_i(\boldsymbol{e}_2)$ acting on atom i and associated with a planar surface defined by a unit normal vector $\boldsymbol{e}_2$. For simplicity of plotting, the cutoff distance used in the figure is equal to $1.75a_l$, where a_l is the lattice distance, although a larger cutoff distance (e.g., $\geq 2.5a_l$) may be needed in real applications for accurate stress analysis. The red dashed line represents a planar surface shifted above atom i by a distance equal to one-half of the atomic plane distance (i.e., $0.25a_l$) so that no atom crosses the surface as a result of thermal vibration. Only the interatomic forces whose trajectories cross the plane surface (the atoms connected by solid lines in Fig. 1) are included in the calculation of the traction vector. Due to the periodicity of the crystal structure, the dimension of the planar surface is an integer multiple of a_l. Although a smaller surface area is locally more descriptive, a larger surface area yields relatively smoother stress distributions. The planar surface was also shifted below atom i by a distance equal to $0.25a_l$ and the same procedure was repeated. Finally, the traction vector acting on atom i was calculated by averaging the resultant tractions on the two planar surfaces placed above and below atom i. For each atom, three traction vectors associated with orthogonal directions $\boldsymbol{e}_1$, $\boldsymbol{e}_2$, and $\boldsymbol{e}_3$, which are aligned with the [100], [010], and [001] crystal directions, were computed and the local stress was directly calculated from the components of the obtained traction vector. When calculating the stress of atoms close to the boundaries, the planar surface may extend outside the structure. In this case, only the surface area inside the structure was considered in the stress analysis. To eliminate the effect of noise induced by atomic thermal vibration, the traction vectors were averaged over a number of time steps. Because of the randomness of thermal vibration, the atomic forces whose trajectories crossed the edges of the planar surfaces were included in the traction vector statistical calculation for 50% of the corresponding time steps, whereas the forces whose trajectories crossed a corner of the planar surfaces were used in the statistical calculation of the traction vector for 25% of these time steps. As shown below, the present stress is equivalent to the classical virial stress in the bulk of FCC and BCC crystalline solids; however, contrary to the classical virial stress, the out-of-plane stress components obtained with the present stress definition diminish at traction-free boundaries. A limitation of the proposed stress method is that the deformation must be relatively small so that the crystal structure is not grossly distorted; otherwise a planar surface may not be defined.

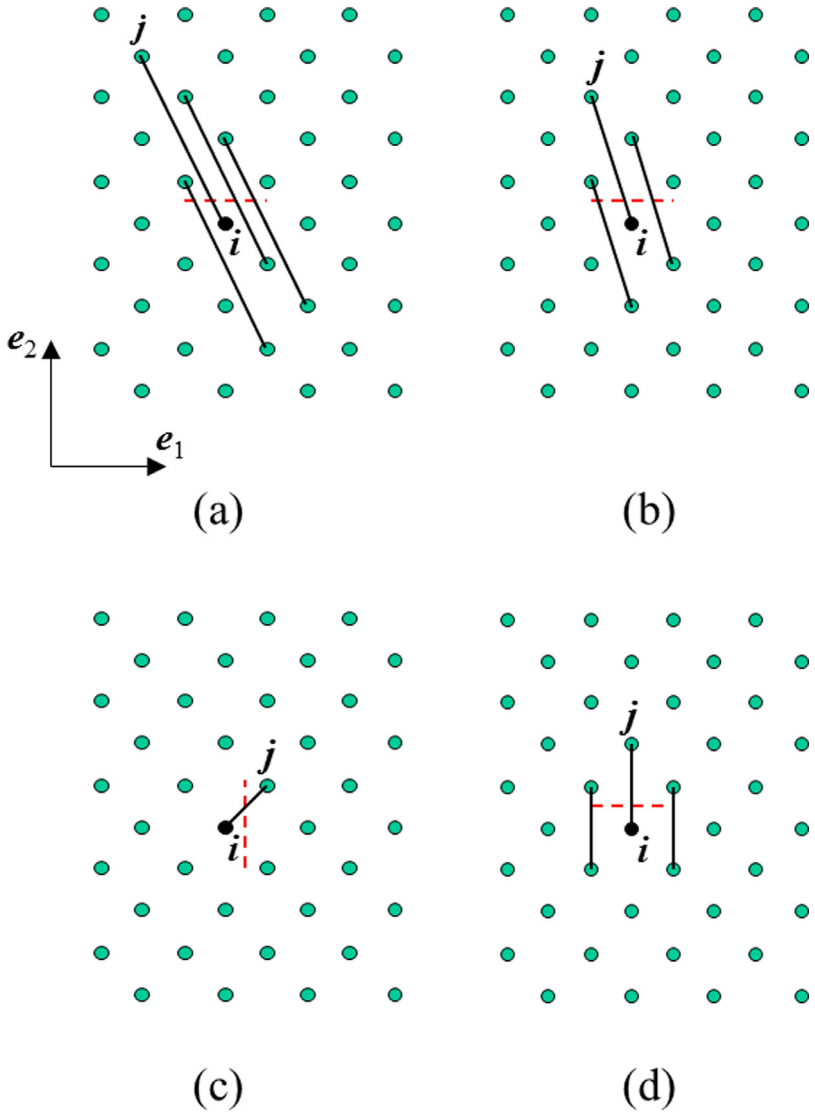

Fig. 2. Examples showing the number of atom pairs N_{ij}^b that generate interatomic forces of the same magnitude and direction as the force F_{ij}^a acting between atoms i and j and passing through a finite plane: (a) $N_{ij}^2 = 4$, (b) $N_{ij}^2 = 3$, (c) $N_{ij}^1 = 1$, and (d) $N_{ij}^2 = 2$. The red dashed line represents the geometrical plane used to define the atomic stress.

The accuracy of the calculated stress may decrease if the crystal structure is severely distorted and/or high stress gradients develop in the deformed solid.

While the energy-based and traction vector-based stress approaches differ in derivation, it will be shown that under certain conditions they are equivalent. From Eqs. (6) and (7) it follows that the stress acting on atom i is given by

$$\sigma_i^{ab} = -\frac{1}{v_i}\sum_{j\neq i} F_{ij}^a r_{ij}^b. \tag{8}$$

Considering small deformation of a single-crystal material with a lattice distance a_l, the volume v_i associated with an atom is given by $v_i = {a_l}^3/4$ (FCC material) or $v_i = {a_l}^3/2$ (BCC material). Therefore, Eq. (8) can be rewritten as

$$\sigma_i^{ab} = -\frac{1}{{a_l}^2}\sum_{j\neq i} F_{ij}^a \frac{r_{ij}^b}{a_l/4} \qquad \text{(FCC material)} \tag{9a}$$

and

$$\sigma_i^{ab} = -\frac{1}{{a_l}^2}\sum_{j\neq i} F_{ij}^a \frac{r_{ij}^b}{a_l/2} \qquad \text{(BCC material)}. \tag{9b}$$

Let's define

$$N_{ij}^b \equiv \frac{r_{ij}^b}{a_l/4} \qquad \text{(FCC material)} \tag{10a}$$

and

$$N_{ij}^b \equiv \frac{r_{ij}^b}{a_l/2} \qquad \text{(BCC material)}. \tag{10b}$$

For a given plane with dimensions $a_l \times a_l$ and normal vector $\boldsymbol{e}_b$ ($b = 1$, 2, or 3) and negligibly small thermal vibrations, it can be shown that N_{ij}^b represents the number of atom pairs with interatomic forces of magnitude and direction the same as those of the force $\boldsymbol{F}_{ij}$ acting between atoms i and j and intersecting the plane surface. Fig. 2 shows examples of the calculation of N_{ij}^b for a 2D FCC crystal structure. As shown in Fig. 2(a), $N_{ij}^2 = 4$. In the traction vector-based approach, all forces generated by the four atomic pairs shown in this figure are included in the stress calculation, whereas in the energy-based approach only the interatomic force between atoms i and j is included in the stress calculation. This is because only the forces applied to atom i are used in Eq. (8) to calculate the atomic stress. Figs. 2(b) and (c) show examples where

$N_{ij}^2 = 3$ and $N_{ij}^1 = 1$, respectively, whereas Fig. 2(d) shows an example where $N_{ij}^2 = 2$. In Fig. 2(d), one-half of the interatomic forces acting along the two solid lines crossing the edges of the plane surface is included in the calculation of the traction vector acting on atom i. As shown below, in the energy-based approach, the force applied between atoms i and j is multiplied by N_{ij}^b. Therefore, the effective force in the energy-based approach is equal to the sum of the forces whose trajectories cross the $a_l \times a_l$ surface area in the traction vector-based approach.

The effective force acting on atom i obtained from the energy-based approach is defined as

$$F_i^{ab} \equiv -\sum_{j\neq i} F_{ij}^a \frac{r_{ij}^b}{a_l/4} = -\sum_{j\neq i} F_{ij}^a N_{ij}^b \qquad \text{(FCC material)} \tag{11a}$$

and

$$F_i^{ab} \equiv -\sum_{j\neq i} F_{ij}^a \frac{r_{ij}^b}{a_l/2} = -\sum_{j\neq i} F_{ij}^a N_{ij}^b \qquad \text{(BCC material)}. \tag{11b}$$

If P_b^i is the set of all atom pairs with forces whose trajectories cross the $a_l \times a_l$ surface area (defined by the normal unit vector $\mathbf{e}_b$) associated with atom i, it follows that

$$\sum_{j\neq i} F_{ij}^a N_{ij}^b = \sum_{(k,j)\in P_b^i} F_{kj}^a.$$

Thus, the atomic stress is given by

$$\sigma_i^{ab} = \frac{F_i^{ab}}{a_l^2} = -\frac{\sum_{(k,j)\in P_b^i} F_{kj}^a}{a_l^2}. \tag{12}$$

Eq. (12) shows that, for FCC and BCC materials, the stress definitions given by Eqs. (5) and (8) are equivalent to that derived from the traction vector-based analysis, provided the material undergoes small deformation and thermal effects are secondary. However, because the equivalence between the two stress definitions may not hold in regions close to the boundaries (e.g., stress-free surfaces) due to the lack of atoms at the outer sides of the system, the equivalence is limited to the bulk of crystalline solids. It is also noted that although the foregoing derivation is for FCC and BCC solids, a similar approach can be followed for most other crystal solids.

4. Results and discussion

In this section, the validity of the atomic stress method introduced in the previous section is demonstrated in the light of MD simulation results of FCC copper-like material with $a_l = 3.603$ Å and Morse potential parameters $D = 0.3429$ eV, $r_0 = 2.866$ Å, and $\alpha = 1.3588$ Å, and diamond tip with $a_l = 3.567$ Å and LJ potential parameters $\varepsilon = 0.002413$ eV and $\sigma = 3.4$ Å. These values of the parameters used in the Morse and LJ potential functions are quoted from the literature (Torrens, 1972; Komvopoulos and Yan, 1997). Unless otherwise stated, in the following MD simulations, the size of the planar surface used to define the atomic stress is $2a_l \times 2a_l$, the cutoff distance for atomic force calculation is $2.5a_l$, and the temperature is set at 0.3 K so that thermal effects are secondary, thermal expansion can be ignored, and the atoms close to the boundary can still reach equilibrium. The desired temperature was maintained by directly scaling the atomic velocity and keeping the total kinetic energy equal to $(3/2)NkT$, where N is the number of atoms in the system, k is Boltzmann's constant, and T is the temperature. All of the simulations were performed with a modified version of the classical MD code LAMMPs (Komvopoulos and Yan, 1997).

4.1. Validation of the stress method

4.1.1. Bulk modulus

The bulk modulus of single-crystal copper was obtained from MD simulations, using Eq. (12) to compute the hydrostatic stress and the change in lattice distance to calculate the volume change. Fig. 3 shows the initial crystal structure of the copper-like MD model used in these simulations. A periodic boundary condition was applied to all the free surfaces of the model. Because of this boundary condition, the initial atom positions are the equilibrium positions. The hydrostatic stress $\sigma_m = (\sigma_{11} + \sigma_{22} + \sigma_{33})/3$ was calculated for different lattice distances. The variation of the lattice distance affects both the hydrostatic stress and the volume. The bulk modulus is defined as $K = \sigma_m/\varepsilon_v$, where ε_v is the dilatation strain defined by $\varepsilon_v = \varepsilon_{11} + \varepsilon_{22} + \varepsilon_{33}$. For the given deformation, $\varepsilon_v = 3(a_l - a_0)/a_0$, where a_0 is the lattice distance at zero hydrostatic stress. Fig. 4 shows the hydrostatic stress σ_m as a function of dilatation strain ε_v. The MD data show a perfect linear fit with a slope $K = 139.8$ GPa, which is very close to the value (137.6 GPa) quoted from the literature for single-crystal copper (Kaye and Laby, 1986).

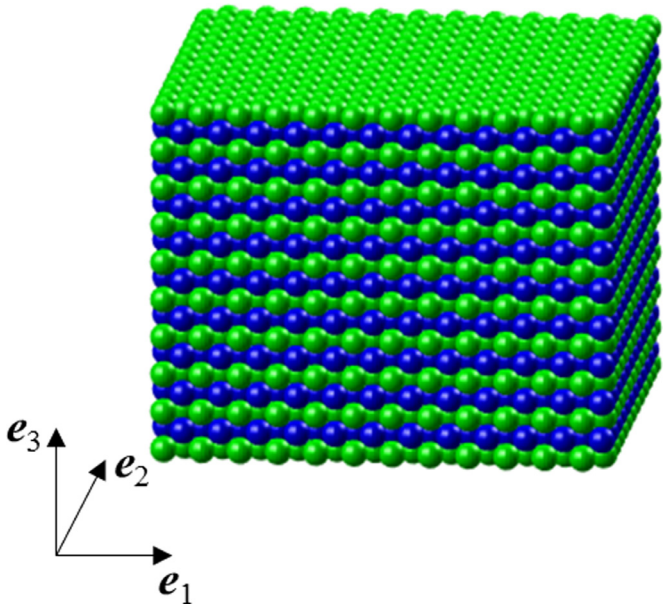

Fig. 3. Initial atomic configuration of an FCC solid. Sequential atomic planes are colored green and blue for clarity.

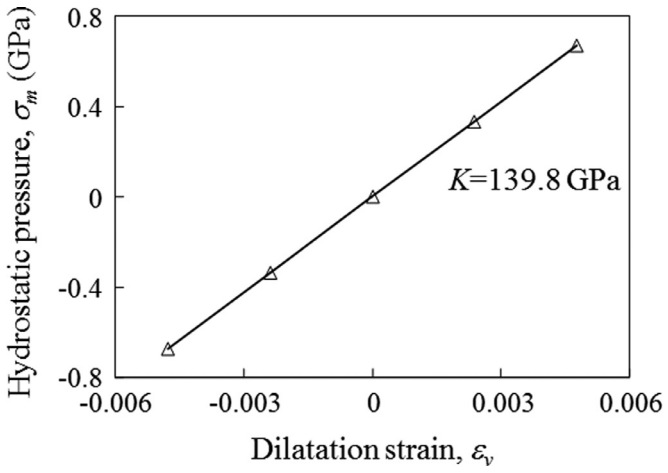

Fig. 4. Hydrostatic stress σ_m versus dilatation strain ε_v for an FCC solid.

4.1.2. Surface tension

Surface tension is a well-known phenomenon that can be studied by considering the shape of droplets and bubbles on solid surfaces. This phenomenon is attributed to the cohesive forces acting between molecules and atoms. Different from bulk atoms, surface atoms are not fully surrounded by atoms and, therefore, tend to cohere more strongly to each other. Likewise, because atoms at solid surfaces lack neighboring atoms, they tend to cohere to each other more strongly than bulk atoms.

An MD model of a copper-like single-crystal structure with a (100) free surface, similar to that used in the MD simulation of the bulk modulus (Fig. 3), was used to simulate surface tension. However, in this simulation the periodic boundary condition was applied only to the four lateral surfaces of the model, while the atoms of the five bottom planes were fixed. The lattice distance a_0 in the original atomic configuration was selected to yield zero stress components at all bulk atoms at a temperature of 0.3 K. The original separation between all neighboring (100) atomic planes was equal to $0.5a_0$. This MD simulation comprised two stages: an equilibrium stage consisting of 20,000 steps during which the copper atoms reached equilibrium and a subsequent deformation stage wherein the resulting stresses were calculated and averaged. At the end of the equilibration stage, the distance between neighboring atomic planes was found to slightly differ from the original setting ($0.5a_0$).

Fig. 5 shows the distance d between adjacent atomic planes normalized by the initial lattice distance a_0 versus the number of atomic plane n, where $n = 1$ corresponds to the atomic plane at the surface. The distance between the two top atomic planes is equal to $\sim 0.55a_0$. The larger distance is attributed to the lack of balancing atoms from directly above, which, if existed, would have forced these atoms back to their originally assigned positions. The variation of the in-plane normal stress σ_{11} normalized by D/r_0^3 with the number of atomic plane n (i.e., the distance from the top atomic layer) is shown in Fig. 6. Because of symmetry, a similar trend was observed with the in-plane stress σ_{22}. A tensile σ_{11} stress develops at the top four atomic planes, with the maximum tensile stress occurring at the free surface. The tensile σ_{11} stress decreases sharply with the distance from the free surface and eventually vanishes at a depth corresponding to the fifth atomic plane. The shear σ_{13} stress and the out-of-plane σ_{33} stress were found to be nearly zero throughout the structure, even close to the surface. Thus, the present stress definition correctly captures the existence of surface tension.

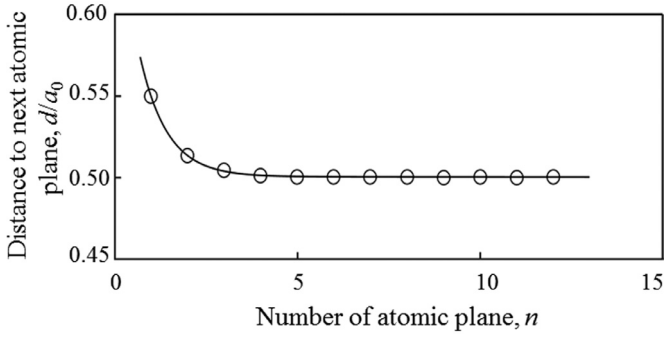

Fig. 5. Dimensionless distance between neighboring atomic plane d/a_0 versus number of atomic plane n for an FCC solid with a (100) free surface.

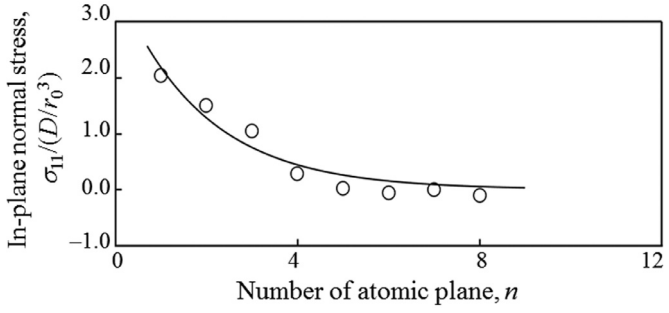

Fig. 6. Dimensionless in-plane normal stress $\sigma_{11}/(D/r_0^3)$ versus number of atomic plane n for an FCC solid with a (100) free surface.

4.2. Contact deformation

MD simulation results of an FCC copper-like substrate indented by a diamond tip are presented in this section. The initial atomic structures of the substrate and the indentation tip are shown in Fig. 7. For simplicity, the diamond tip is modeled as a prismatic rigid punch with a flat end. Bulk atom interaction is described by the Morse potential (Eq. (3)), whereas tip-substrate atom interaction is described by the LJ potential (Eq. (4)). Similar to the surface tension simulation, a periodic boundary condition was applied to the four vertical surfaces of the substrate, while all the atoms of the bottom planes were fixed. The surface separation and tip-substrate interference are defined in Fig. 8. To prevent severe distortion of the substrate structure, the maximum interference distance δ was set equal to $0.57a_0$. This simulation comprised an equilibrium stage with 20,000 time steps followed by an indentation stage. The number of time steps used in the indentation stage depends on the initial surface separation, interference distance, and indentation speed, which was fixed at 5 m/s in this simulation. After the indentation stage, the stresses were calculated and averaged.

Normalized stress distributions along the surface line AA′ that passes through the center of contact (Fig. 7) are shown in Fig. 9. Outside the contact region, σ_{33} and σ_{13} vanish, whereas σ_{11} is tensile due to the effect of surface tension. Within the contact region, both σ_{11} and σ_{33} are compressive, with the maximum normal stresses occurring close to the contact edge, in qualitative

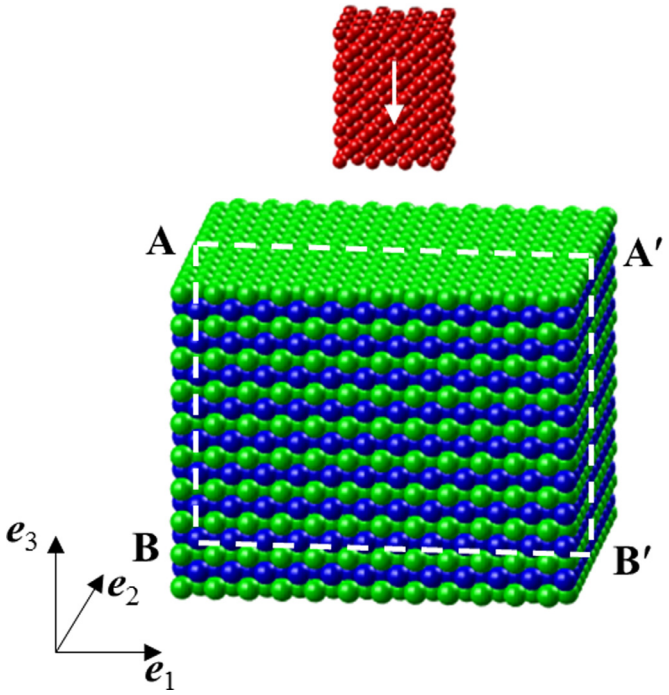

Fig. 7. Initial atomic configurations of an FCC substrate and a prismatic diamond tip. Sequential atomic planes are colored green and blue for clarity.

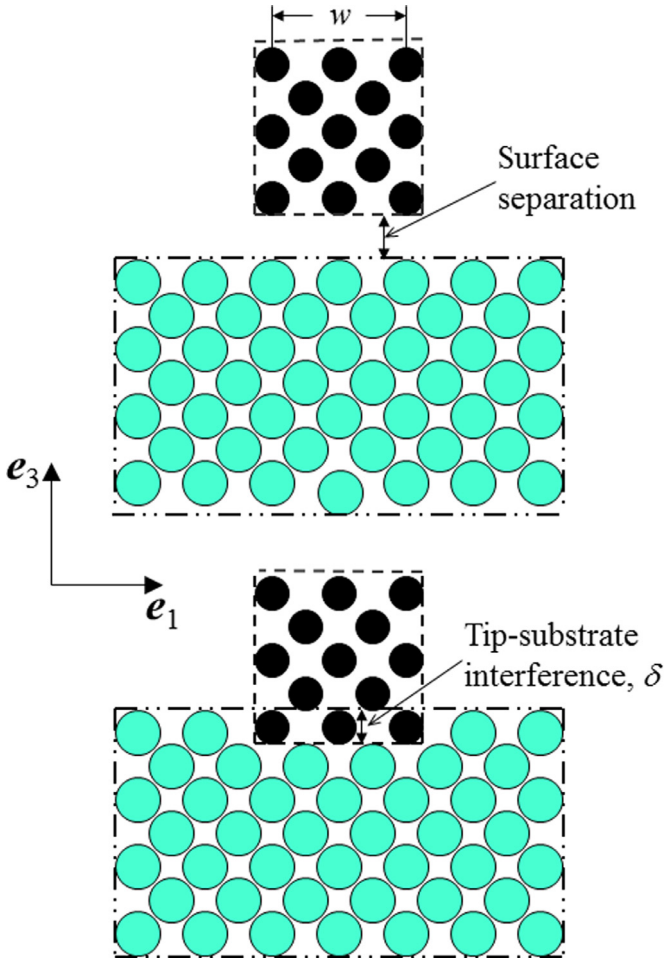

Fig. 8. Definition of surface separation (top) and tip-substrate interference (bottom).

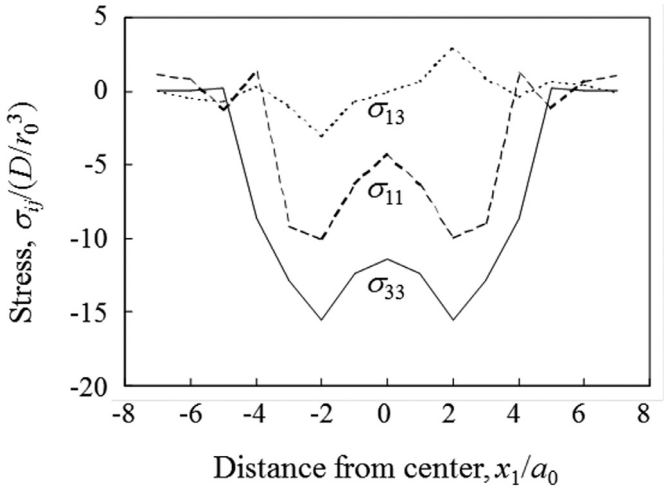

Fig. 9. Distributions of dimensionless surface stresses $\sigma_{ij}/(D/r_0^3)$ ($i, j = 1, 2$, or 3) versus distance x_1/a_0 along the line AA′ passing through the center of contact (Fig. 7) for a tip-substrate interference distance $\delta = 0.57a_0$, where a_0 is the lattice distance of the undeformed structure.

agreement with the classical solution of an elastic half-space compressed by a rigid flat punch (Johnson, 1985). The σ_{13} stress is antisymmetric and reaches a maximum near the contact edge. The accuracy of the stresses close to the contact edge may be affected by high stress gradients, localized lattice distortion, and thermal noise, which were minimal in the present simulation.

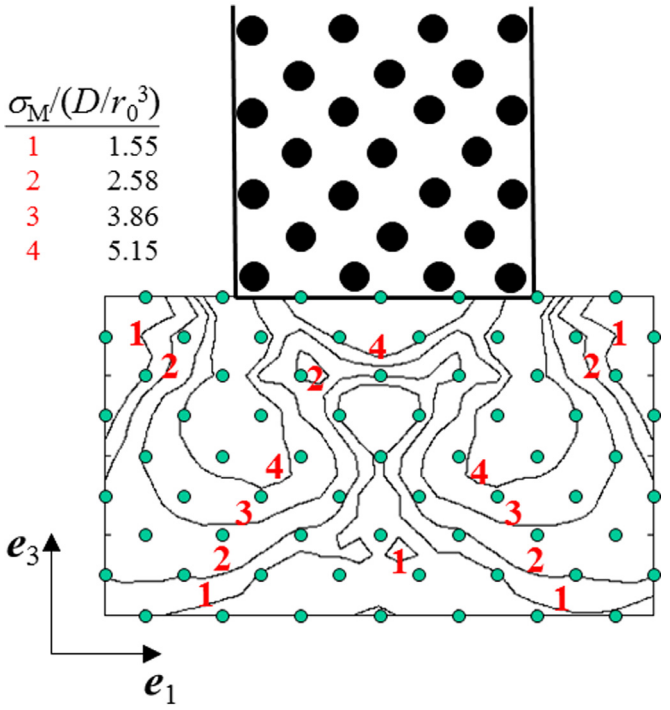

Fig. 10. Contours of dimensionless von Mises equivalent stress $\sigma_M/(D/r_0^3)$ on plane (AA′B′B) (Fig. 7) for a tip-substrate interference distance $\delta = 0.57a_0$, where a_0 is the lattice distance of the undeformed structure.

Fig. 10 shows contours of the von Mises equivalent stress σ_M normalized by D/r_0^3 on the plane (AA′B′B) (Fig. 7). The atomic stress is higher at the contact edge than at the center of contact. The stress contours shown in Fig. 10 are similar to the 2D photoelastic fringe patterns generated in an elastic medium by an indenting rigid flat punch (Johnson, 1985), except for the nonzero surface stress outside the contact region, which is due to the effect of surface tension that is not captured in the CM analysis.

5. Conclusions

A traction vector-based stress analysis for MD systems was introduced in this study and its equivalence to an energy-based approach was proven for the bulk of FCC and BCC crystalline solids subjected to small deformation and thermal vibration. The validity of the present stress method was verified by simulation results of the bulk modulus, surface tension, and indentation stress field of an FCC copper-like solid. Based on the presented analysis, simulation results, and discussion, the following main conclusions can be drawn from this study.

(1) The atomic stress method of this study is applicable to both FCC and BCC solids, including the region adjacent to the free surface where the classical virial stress does not satisfy the traction-free boundary condition.
(2) The bulk modulus of an FCC copper-like material calculated based on the present atomic stress definition is very close to that quoted from the literature.
(3) The phenomenon of surface tension is correctly captured by the present stress method, confirming the development of an in-plane tensile stress in the near-surface region of a single-crystal solid, which is not captured by the classical virial stress and CM analyses.
(4) MD simulations of an FCC substrate with its (100) free surface in contact with a prismatic flat diamond tip yielded a subsurface stress field similar to that of classical CM contact

analysis, with the exception of a nonzero normal stress outside the contact region of the MD model cuased by surface tension.

Credit author statement

JY performed all the MD simulations, implemented the MD code, and wrote the first draft of the paper. KK formulated the objectives of the study, supervised the research of JY, and wrote the final draft of the paper. Both authors edited and revised the final manuscript.

Declaration of Competing Interest

The authors declare that they have no known competing financial interests or personal relationships that could have appeared to influence the work reported in this paper.

References

Belak, J., Stowers, I.F., 1990. Molecular dynamics studies of surface indentation in two dimensions. Mater. Res. Soc. Symp. Proc. 193, 259–264.

Belak, J., Stowers, I.F., 1992. The indentation and scraping of a metal surface: a molecular dynamics study. In: Singer, I.L., Pollock, H.M. (Eds.), Fundamentals of Friction: Macroscopic and Microscopic Processes. Kluwer Academic Publishers, The Netherlands, pp. 511–520.

Born, M., Huang, K., 1954. Dynamical Theory of Crystal Lattices. Clarendon Press, Oxford, UK, pp. 129–165.

Chen, X., Lu, S., Zhao, Y., Fu, T., Huang, C., Peng, X., 2018. Molecular dynamic simulation on nano-indentation of NiTi SMA. Mater. Sci. Eng. A 712, 592–602.

Cheung, K.S., Yip, S., 1991. Atomic-level stress in an inhomogeneous system. J. Appl. Phys. 70, 5688–5690.

Clausius, R., 1870. On a mechanical theorem applicable to heat. Philo. Mag. 40, 122–127.

Egami, T., Srolovitz, D., 1982. Local structural fluctuations in amorphous and liquid metals: a simple theory of the glass transition. J. Phys. F: Met. Phys. 12, 2141–2163.

Eggen, B.R., Johnston, R.L., Li, S., Murrell, J.N., 1992. Potential energy functions for atomic solids IV. Reproducing the properties of more than one solid phase. Mol. Phys. 76, 619–633.

Foiles, S.M., Baskes, M.I., Daw, M.S., 1986. Embedded-atom-method functions for the fcc metals Cu, Ag, Au, Ni, Pd, Pt, and their alloys. Phys. Rev. B 33, 7983–7991.

Hoover, W.G., Hoover, C.G., Stowers, I.F., Siekhaus, W.J., 1989. Interface tribology via nonequilibrium molecular dynamics. Mater. Res. Soc. Symp. Proc. 140, 119–124.

Johnson, K.L., 1985. Contact Mechanics. Cambridge University Press, Cambridge, UK, p. 103.

Kallman, J.S., Hoover, W.G., Hoover, C.G., de Groot, A.J., Lee, S.M., Wooten, F., 1993. Molecular dynamics of silicon indentation. Phys. Rev. B 47, 7705–7709.

Kaye, G.W.C., Laby, T.H., 1986. Tables of Physical and Chemical Constants and Some Mathematical Functions. Longman, New York, NY.

Komanduri, R., Chandrasekaran, N., Raff, L.M., 2000. Molecular dynamics simulation of atomic-scale friction. Phys. Rev. B 61, 14007–14019.

Komvopoulos, K., Yan, W., 1997. Molecular dynamics simulation of single and repeated indentation. J. Appl. Phys. 82, 4823–4830.

Landman, U., Luedtke, W.D., Burnham, N.A., Colton, R.J., 1990. Atomistic mechanisms and dynamics of adhesion, nanoindentation, and fracture. Science 248, 454–461.

Leng, Y., Yang, G., Hu, Y., Zheng, L., 2000. Computer experiments on nano-indentation: a molecular dynamics approach to the elasto-plastic contact of metal copper. J. Mater. Sci. 35, 2061–2067.

Love, A.E.H., 1944. A Treatise on the Mathematical Theory of Elasticity. Dover, New York, NY.

Luan, B., Robbins, M.O., 2005. The breakdown of continuum models for mechanical contacts. Nature 435, 929–932.

Nielsen, O.H., Martin, R.M., 1985. Quantum-mechanical theory of stress and force. Phys. Rev. B 32, 3780–3791.

Saether, E., Hochhalter, J.D., Glaessgen, E.H., Mishin, Y., 2014. Multiscale analysis of structurally-graded microstructures using molecular dynamics, discrete dislocation dynamics and continuum crystal plasticity. NASA/TM-2014-218265.

Sansoz, F., 2011. Atomistic processes controlling flow stress scaling during compression of nanoscale face-centered-cubic crystals. Acta Mater. 59, 3364–3372.

Scagnetti, P.A., Nagem, R.J., Sandri, G.V.H., Bifano, T.G., 1996. Stress and strain analysis in molecular dynamics simulation of solids. ASME J. Appl. Mech. 63, 450–452.

Shimada, T., Ouchi, K., Chihara, Y., Kitamura, T., 2015. Breakdown of continuum fracture mechanics at the nanoscale. Sci. Rep. 5, 8596.

Solhjoo, S., Vakis, A.I., 2015. Single asperity nanocontacts: comparison between molecular dynamics simulations and continuum mechanics models. Comput. Mater. Sci. 99, 209–220.

Srinivasan, P., Nicola, L., Simone, A., 2018. Atomistic modeling of the orientation-dependent pseudoelasticity in NiTi: tension, compression, and bending. Comput. Mater. Sci. 154, 25–36.

Stukowski, A., 2012. Structure identification methods for atomistic simulations of crystalline materials. Model. Simul. Mater. Sci. Eng. 20, 045021.

Stukowski, A., Albe, K., Farkas, D., 2010. Nanotwinned fcc metals: strengthening versus softening mechanisms. Phys. Rev. B 82, 224103.

Subramaniyan, A.K., Sun, C.T., 2008. Continuum interpretation of virial stress in molecular simulations. Int. J. Solids Struct. 45, 4340–4346.

Torrens, I.M., 1972. Interatomic Potentials. Academic Press, New York, NY.

Tsai, D.H., 1979. The virial theorem and stress calculation in molecular dynamics. J. Chem. Phys. 70, 1375–1382.

Vitek, V., Egami, T., 1987. Atomic level stresses in solids and liquids. Phys. Stat. Sol. B 144, 145–156.

Wang, B., Kang, G., Kan, Q., Zhou, K., Yu, C., 2017. Molecular dynamics simulations to the pseudo-elasticity of NiTi shape memory alloy nano-pillar subjected to cyclic compression. Comput. Mater. Sci. 131, 132–138.

Yan, W., Komvopoulos, K., 1998. Three-dimensional molecular dynamics analysis of atomic-scale indentation. ASME J. Tribol. 120, 385–392.

Yang, J., Komvopoulos, K., 2005. A molecular dynamics analysis of surface interference and tip shape and size effects on atomic-scale friction. ASME J. Tribol. 127, 513–521.

Zepeda-Ruiz, L.A., Stukowski, A., Oppelstrup, T., Bulatov, V.V., 2017. Probing the limits of metal plasticity with molecular dynamics simulations. Nature 550, 492–495.

Zhang, L., Jasa, J., Gazonas, G., Jérusalem, A., Negahban, M., 2015. Extracting continuum-like deformation and stress from molecular dynamics simulations. Comput. Meth. Appl. Mech. Eng. 283, 1010–1031.

Zhou, M., 2003. A new look at the atomic level virial stress: on continuum-molecular system equivalence. Proc. R. Soc. Lond. A 459, 2347–2392.